Computer Methods in Biomechanics and Biomedical Engineering, 2015
Vol. 18, No. 7, 711–720, http://dx.doi.org/10.1080/10255842.2013.843675

Taylor & Francis
Taylor & Francis Group

Finite element analysis of *pectus carinatum* surgical correction via a minimally invasive approach

Sara C. Neves[a,b], ACM Pinho[c], Jaime C. Fonseca[d], Nuno F. Rodrigues[e], Tiago Henriques-Coelho[f], Jorge Correia-Pinto[a] and João L. Vilaça[a,g]*

[a]*ICVS/3B's – PT Government Associate Laboratory, Life and Health Sciences Research Institute (ICVS), School of Health Sciences, University of Minho, 4710-057 Braga, Portugal;* [b]*INEB – Instituto de Engenharia Biomédica, Universidade do Porto, Rua do Campo Alegre, 823, 4150-180 Porto, Portugal;* [c]*CT2M – Centre for Mechanical and Materials Technologies, University of Minho, 4800-058 Guimarães, Portugal;* [d]*Algoritmi Research Centre, University of Minho, 4800-058 Guimarães, Portugal;* [e]*HASLab/INESC TEC, University of Minho, Braga, Portugal;* [f]*Department of Pediatric Surgery, São João Hospital, Porto, Portugal;* [g]*DIGARC – Digital Games Research Centre, Polytechnic Institute of Cávado and Ave (IPCA), Campus IPCA, 4750-810 Barcelos, Portugal*

(*Received 13 December 2012; accepted 9 September 2013*)

Pectus carinatum (PC) is a chest deformity caused by a disproportionate growth of the costal cartilages compared to the bony thoracic skeleton, pulling the sternum towards, which leads to its protrusion. There has been a growing interest on using the 'reversed Nuss' technique as a minimally invasive procedure for PC surgical correction. A corrective bar is introduced between the skin and the thoracic cage and positioned on top of the sternum highest protrusion area for continuous pressure. Then, it is fixed to the ribs and kept implanted for about 2–3 years. The purpose of this work was to (a) assess the stresses distribution on the thoracic cage that arise from the procedure, and (b) investigate the impact of different positioning of the corrective bar along the sternum. The higher stresses were generated on the 4th, 5th and 6th ribs backend, supporting the hypothesis of *pectus* deformities correction-induced scoliosis. The different bar positioning originated different stresses on the ribs' backend. The bar position that led to lower stresses generated on the ribs backend was the one that also led to the smallest sternum displacement. However, this may be preferred, as the risk of induced scoliosis is lowered.

Keywords: *pectus carinatum*; finite element analysis; reversed Nuss procedure; minimally invasive approach

1. Introduction

Pectus carinatum (PC) is a deformity of the anterior chest wall involving a variety of protrusion configurations, but most frequently with anterior projection of the mid and lower sternum and adjacent costal cartilages (Brodkin 1958). It is a general consensus that, like *pectus excavatum* (PE), PC origins from a disproportionate growth of the costal cartilages compared to the bony thoracic skeleton; this presses the sternum, leading to its protrusion, depression or a combination of both (Peña et al. 1981). In most PC cases, there is a chest narrowing from side to side, with the ribs projecting more anteriorly and with less curvature than normal, and also a slight sternum rotation, due to different cartilage growth rates on each side of the thoracic cage (Fonkalsrud 2008). The overall prevalence of PC is of 0.6%, being more common in male (4:1, male–female ratio) (Hock 2009).

The classical management of both PC and PE has been primarily surgical (Singh 1980; Fonkalsrud et al. 2000; Fonkalsrud and Beanes 2001); it generally consists of a modification of the Ravitch technique, on which the deformed costal cartilages are resected, followed by a sternal osteotomy. However, it may result in a worsening of cosmetic results and decreased chest wall compliance over time (Weber 2005). PC can also be corrected using a conservative external orthopaedic treatment using a bracing system, but its effectiveness mainly relies on the patient's will (Coelho and Guimarães 2007).

Focused on a less invasive approach, the 'Nuss procedure' (Nuss et al. 2002) developed for the PE correction uses an internal support bar, aiming to remodel the chest wall cartilage. The plasticity of the chest wall has been demonstrated and led to the hypothesis that, in an analogous way, PC defects would also remodel in response to chronic pressure, leading to an aesthetically superior and less invasive result (Kravarusic et al. 2006). The corrective approach by means of a minimally invasive surgical (MIS) procedure using an internal bar may be preferred to external bracing systems in cases of older patients, due to skeleton maturity and also due to the discomfort associated with the use of braces.

Only more recently, a MIS approach for PC has been investigated (Abramson et al. 2009; Schaarschmidt et al. 2011; Yüksel et al. 2011) based on the Nuss technique, on which the corrective bar is placed under the skin and on top of the sternum highest protrusion point for its continuous compression, and fixed on both sides of the chest wall.

Until now, and conversely to PE (Chang et al. 2008; Wei et al. 2010), no finite element (FE) models-based

*Corresponding author. Email: joaovilaca@ecsaude.uminho.pt

studies were performed regarding the modified Nuss technique for PC correction. The main objectives of this work were (a) a preliminary study of the stresses generated in the thoracic cage resultant from the MIS correction of PC and also (b) the study of different bar positions to assess the impact of this choice on thoracic cage reaction.

2. Methods

2.1 Patient-specific thoracic cage FE model

For simulation purposes, a simplified thoracic cage structure was used. Based on Awrejcewicz and Łuczak (2006) and Chang et al.'s (2008) works, the following simplifications were used:

- the anatomic model consisted only of the ribs (divided in cortical and trabecular bone), sternum and costal cartilage due to their major contribution to the thoracic cage integrity, therefore neglecting the soft tissues (e.g. intercostal muscles, internal organs) (Awrejcewicz and Łuczak 2006) and
- based on clinical observations, the spinal structure does not significantly change immediately after the Nuss procedure in the PE correction (Chang et al. 2008); considering that the modified Nuss procedure for the PC correction has a similar non-immediate impact on the spine, the same was assumed in this study, and therefore it was not included in the model.

The thorax of a 14-year-old male patient with PC was scanned using computer tomography (CT) (Siemens® SOMATOM Sensation Cardiac 64, 120 kVp, 0.615 mm × 0.615 mm × 1.000 mm voxel resolution and 315 mm × 315 mm × 373 mm volume size). Informed consent was obtained from the guardian of the patient for the use of the CT data and this study was approved by the hospital and research institute ethics committee.

A volumetric mesh of the rib cage suitable for FE analysis was generated from the DICOM CT images using iso2mesh version 1.0 by Fang and Boas (2009), a 3D surface and volumetric mesh generator toolbox for MATLAB (MathWorks, MA, USA). First, the image data-set was resampled from 0.615 mm × 0.615 mm × 1 mm to 1 mm × 1 mm × 1 mm for further mesh generation simplification. After this, a semi-automated segmentation was performed to generate the volumes (binary volumes) of four different structures – ribs cortical bone, ribs trabecular bone, costal cartilages and sternum – based on image density thresholding of different greyscale intensities. The volumetric meshes of each anatomic part were then generated, consisting of four-node isoparametric tetrahedral (C3D4) elements and consequently a rib cage structure for the PC corrective procedure biomechanical simulation was obtained. For the FE model accuracy verification, the volumetric meshes surfaces were compared to each structure outer contours in the original CT images.

2.2 Corrective bar FE model

A bar model based on the i3DExcavatum bar (iSurgical3D, Guimarães, Portugal) was designed using the computer-aided design (CAD) software Solidworks® (SolidWorks Corp., Concord, MA, USA). It consists of a bar with embedded stabilizers (Figure 1(a)); both sides can be fixed to the ribs using suture wires. Using the patient's CT data, an automatically generated personalized bar template was obtained using the software developed by Vilaça et al. (2009). It selects the size and shape of the corrective bar, and performs its automatic bending for PE and PC repair according to the patient thoracic morphology. Based on pre-operative chest CT-scan, the software first performs a 3D reconstruction of the thoracic cage. After this, and for PC, it detects the highest point of the sternum (HPS), the mid-axillaries lines and the horizontal body plan that includes the HPS. With this information and assuming a corrective position – sternum placed at the same level of the highest ribs(s) – it calculates the most appropriate size and generates a virtual model of the corrective bar. As the corrective bar personalized bending is based on the patient's anatomy and performed before and not during surgery, it diminishes the surgery time. The corrective bar bending template was then used to generate the 3D bended bar model using Solidworks (Figure 1(b)).

2.3 Models assembly

The rib cage model and the corrective bar model were imported into the FE analysis software ABAQUS®/Explicit (Dassault Systèmes, Providence, RI, USA). Here the bar model was positioned parallel to the sternum highest protrusion point, without contacting it (Figure 1); the contact was further established during simulation.

For the different corrective bar positioning study, the bar was placed in six different positions. A 5 mm displacement in the *zz*-axis was used, starting from 10 mm below to 20 mm above the position used for the corrective study, considered as the 0 mm position.

2.4 Finite element analysis

The rib cage components and bar materials properties are present in Table 1 (Awrejcewicz and Łuczak 2006; Rack and Qazi 2006; Li et al. 2010). The material chosen for the corrective bar was the titanium alloy Ti–6Al–4V (Rack and Qazi 2006). All the structures were treated as isotropic, homogeneous and linear elastic materials.

All contact pairs between anatomic parts were treated as ties: sternum/costal cartilage, costal cartilage/cortical

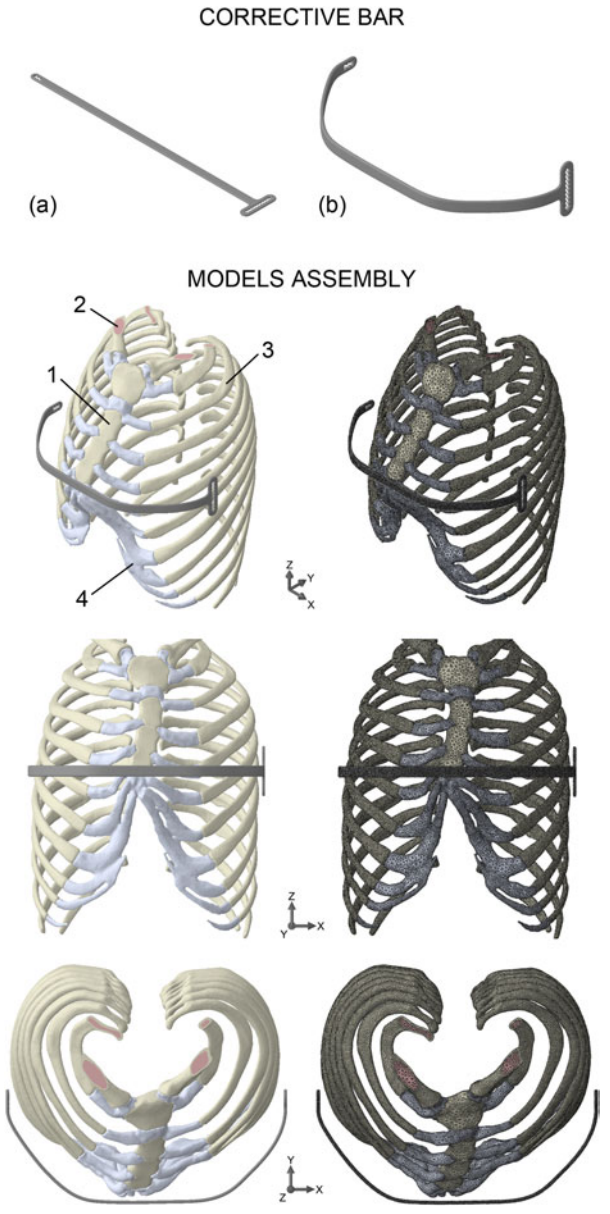

Figure 1. Above: *pectus carinatum* corrective bar model based on the i3DExcavatum bar (iSurgical3D) (a) before and (b) after patient-specific modelling. Below: rib cage and corrective bar models assembly and relative positioning before the simulation study, with visible mesh exterior edges on the right column. The rib cage model is composed by (1) the sternum, (2) the ribs trabecular bone, (3) the ribs cortical bone and (4) the costal cartilages.

bone and cortical bone/trabecular bone. For the interaction between the corrective bar and the rib cage, two different coefficients of friction were used: $\mu = 0.65$ for the titanium alloy/cortical bone interaction (Wei et al. 2010) and $\mu = 0.15$ for the titanium alloy/costal cartilage interaction (Zhou et al. 2005). As aforementioned, the spinal structure was not included in the simulation, but it was used to assess the closest portions of the vertebrae to

Table 1. Rib cage and corrective bar material properties used in the finite element (FE) model.

	ρ (kg/m^3)	E ($\times 10^6$ Pa)	ν	Reference
Cortical bone	2000	11,500.0	0.300	Li et al. (2010)
Trabecular bone	1000	40.0	0.450	Li et al. (2010)
Sternum bone	1000	11,500.0	0.300	Awrejcewicz and Łuczak (2006)
Costal cartilage	1500	24.5	0.400	Awrejcewicz and Łuczak (2006)
Titanium alloy (Ti−6Al−4V)	4429	113,764.0	0.342	Rack and Qazi (2006)

the ribs' backend. Based on this proximity, the ribs' backend surface nodes were constrained as pins (ABAQUS fixed translations and free rotations).

The analysis was divided in three steps. The first step – sternum positioning – consisted of pressing the sternum to an approximate final corrected position. According to the CT data, the approximate distance in the *yy*-axis between the sternum highest protrusion point and the costal cartilages associated with the 11th and 12th ribs is about 50 mm. Therefore, this was the value used for the sternum positioning on the first step. In the second step – bar positioning – the bar was displaced 55 mm on *yy* direction towards the sternum using displacement conditions, in order to simplify the model. The last step consisted on the inactivation of bar displacement, pinning it on both sides of the rib cage, and, at the same time, releasing the sternum from compression. The rib cage then tries to achieve its original position, but the corrective bar prevents this from happening and, consequently, several reaction forces are generated. The large displacement nonlinear solution in the ABAQUS FE analysis software was used to ensure the simulation results accuracy.

A convergence test was performed using the simulated results of seven rib-cage meshes (Table 2); the convergence criterion used was the relative difference of the corrected displacement at the end of the sternum, using a tolerance of 1%. According to the convergence study, the rib cage model used was the one with $E = 584{,}335$ elements and $N = 195{,}922$ nodes.

3. Results

The distribution of the von Mises stress on the rib cage model under the corrective compression was investigated; it is a scalar variable that is defined in terms of all individual stress components and, therefore, a good representative of the state of stresses that has been extensively used in biomechanical studies of bone (Hasan et al. 2011; Jeon et al. 2011; Jorge et al. 2012).

The distributions of the overall stress state for the whole model and each anatomical part are shown under effect of the rib cage reaction after bar lateral pinning (Figures 2 and 3). A qualitative and quantitative analysis was performed based on a progressive visual 13 or 14 colour scale, ranging from dark blue to black or white to black, respectively. For the individual analysis of each rib cage structure, the remaining structures were kept translucent for an easier stress localization and correlation between structures.

3.1 Stress and displacement analysis

The corrective bar prevents the sternum bone from returning to its original position; therefore, the stresses on this bone (Figure 3) are concentrated where the thoracic cage contacts the bar. A correction of the sternum rotation is also visible (Figure 2). The stresses generated in the costal cartilage (Figure 3) are located near the sternum bone and at the region corresponding to the sternum highest displacement. The stresses generated on the ribs (Figure 3) are concentrated mainly on their posterior extremities and, more specifically, on the 4th (higher values – Figure 4), 5th and 6th ribs. The values are higher for the cortical bone when compared to the trabecular bone. The right side of the rib cage also presents higher stress values than the left side.

The magnitude (vectorial resultant) and the different axis maximum displacement values of each structure are present in Table 3. The displacement magnitude distribution presented in Figure 5 shows that the lower part of the sternum and the costal cartilage were the structures that suffered the highest displacement.

3.2 Different corrective bar positioning study

After the corrective procedure simulation, the corrective bar positioning on the *zz*-axis was changed to study its impact on the stresses generated on the ribs' backend and sternum. The corrective bar displacement on the *yy*-axis (55 mm) was maintained for each different bar *zz*-axis position. Figure 6 shows the stresses generated on the ribs' cortical bone and sternum for each corrective bar position. As the 10th, 11th and 12th ribs are not connected to costal cartilages linked to the sternum (Figures 1 and 3), they are not affected by the sternum corrective movement, and thus only the equivalent stresses generated on the 1st to 9th ribs' backend are represented. As it can be observed in Figure 6, the different bar positioning originates different stress distribution both on the ribs and sternum. It is possible to correlate the ribs' cortical bone and sternum-generated stresses in a direct way: when the stress on the sternum increases, the ribs' cortical bone stress decreases and vice versa. However, it is not possible to establish a direct relation between the bar positioning and the increase or decrease of the stresses generated on the ribs and sternum.

Regarding the sternum maximum displacement (SMD) on the *yy*-axis, the main difference verified was ≈6.33 mm (max. $SMD_{-5\,mm} = 44.37$ mm and min. $SMD_{20\,mm} = 38.04$ mm).

The different corrective bar positioning also leads to different contact pressure sites and pressure values on the bar (Figure 7). The costal cartilages and the ribs are the structures that exert the most significant contact pressure values against the bar. Only for the 0 and −5 mm positioning the sternum exerts a contact pressure higher than 0.1×10^6 Pa.

4. Discussion

The simplified rib cage model presented in this work allowed the study of the corrective bar biomechanical effects that cannot be studied clinically with patients with PC. For the PC deformity correction, the bar displacement was used instead of sternum compressive forces as, to our

Table 2. Convergence test of seven rib cage meshes with different number of elements (*E*) and nodes (*N*), using the maximum corrected displacement (in mm) at the end of the sternum: in magnitude (CDM) and considering only the displacement along the *yy*-axis (CDY).

Rib cage		Sternum		Corrected displacement			
				CDM		CDY	
E	*N*	*E*	*N*	(mm)	RD (%)	(mm)	RD (%)
511,118	171,571	9797	3070	41.62		39.01	
540,918	181,514	9837	3086	45.78	9.09	43.26	9.82
584,335	195,922	10,512	3262	45.75	0.07	43.31	0.12
647,967	217,540	11,677	3594	46.11	0.78	43.49	0.41
746,634	270,256	13,404	4062	45.86	0.54	43.41	0.18
897,350	302,823	15,404	4672	46.06	0.43	43.50	0.21
1,173,940	395,401	20,041	5913	46.21	0.32	43.70	0.46

Note: RD, relative difference.

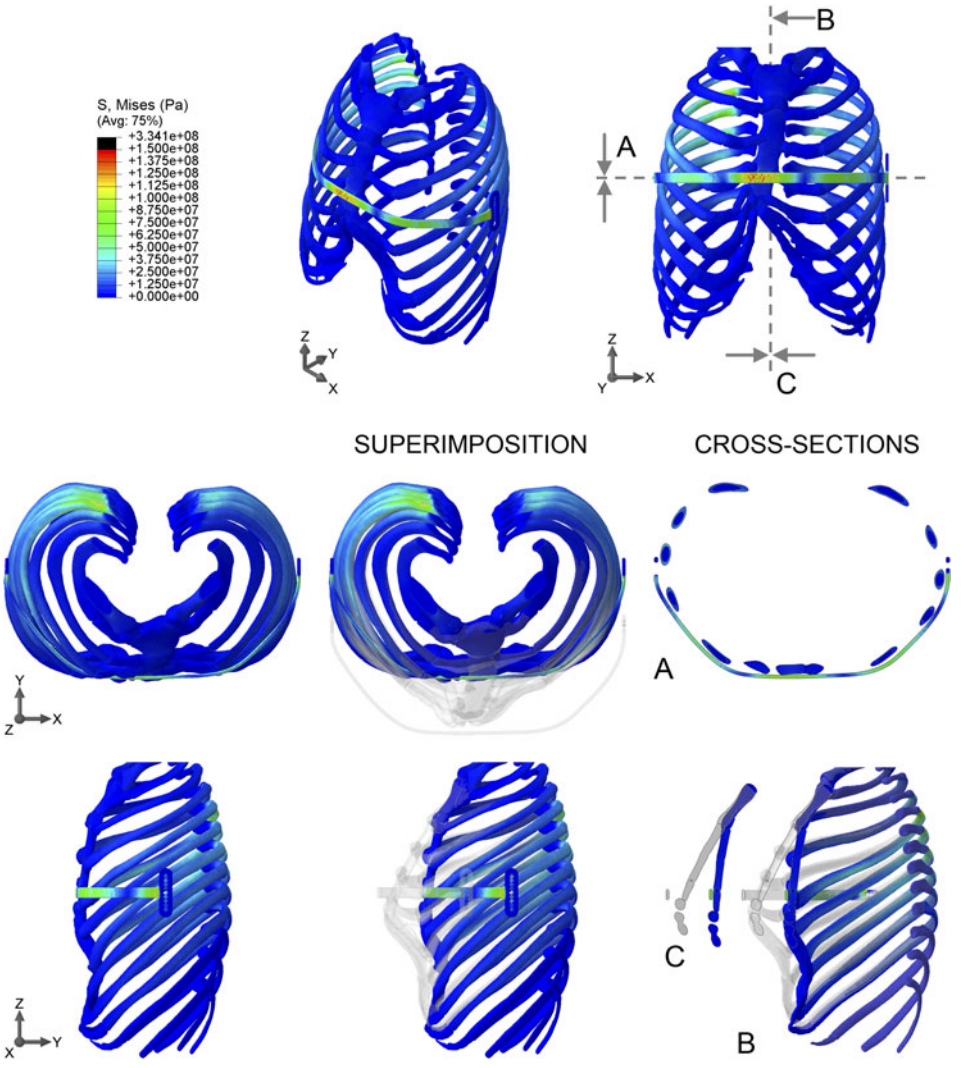

Figure 2. von Mises equivalent stress distribution on the rib cage and on the bar after the corrective procedure simulation, with the before (translucent) and after states superimposition.

knowledge, no information regarding compressive forces values needed for PC correction is available in the literature.

During this MIS procedure, no costal cartilages are removed and, consequently, the force applied to the sternum is transmitted throughout the chest wall in a chain-like reaction. According to Figure 3 and regarding the anatomical structures, a greater stress amount was generated on the posterior extremities of the ribs. This is related to the area where the higher stresses are generated near the sternum: the ribs in which anterior extremities are closer to this sternum region present higher stress values – the 4th, 5th and 6th ribs. In Figure 4, the rib presenting the highest stress – right side 4th rib – is represented along with the left side 4th rib, the sternum and the costal cartilage portions that link them. When the sternum is displaced on the *yy*-axis, the costal cartilage accompanies it and obliges the ribs anterior extremity to move inwards as well. Consequently, the rib's curvature increases (spotted by the $*$) and, along with the generated momentum, the stress concentrates on the rib's posterior extremities which are constrained as pins. As can be seen in Figures 3 and 4, the sternum is slightly deviated to the right side of the rib cage (asymmetrical PC), leading to consequent higher stress values on the ribs of the corresponding side.

Similarly to what happens in the correction of PE, special attention must be paid to these stresses generated near the spine, due to *pectus* deformities correction of mid-/long-term associated scoliosis. According to Waters et al. (1989), the asymmetric pneumatic thoracic pressures and paraspinal muscle imbalances might be the cause of

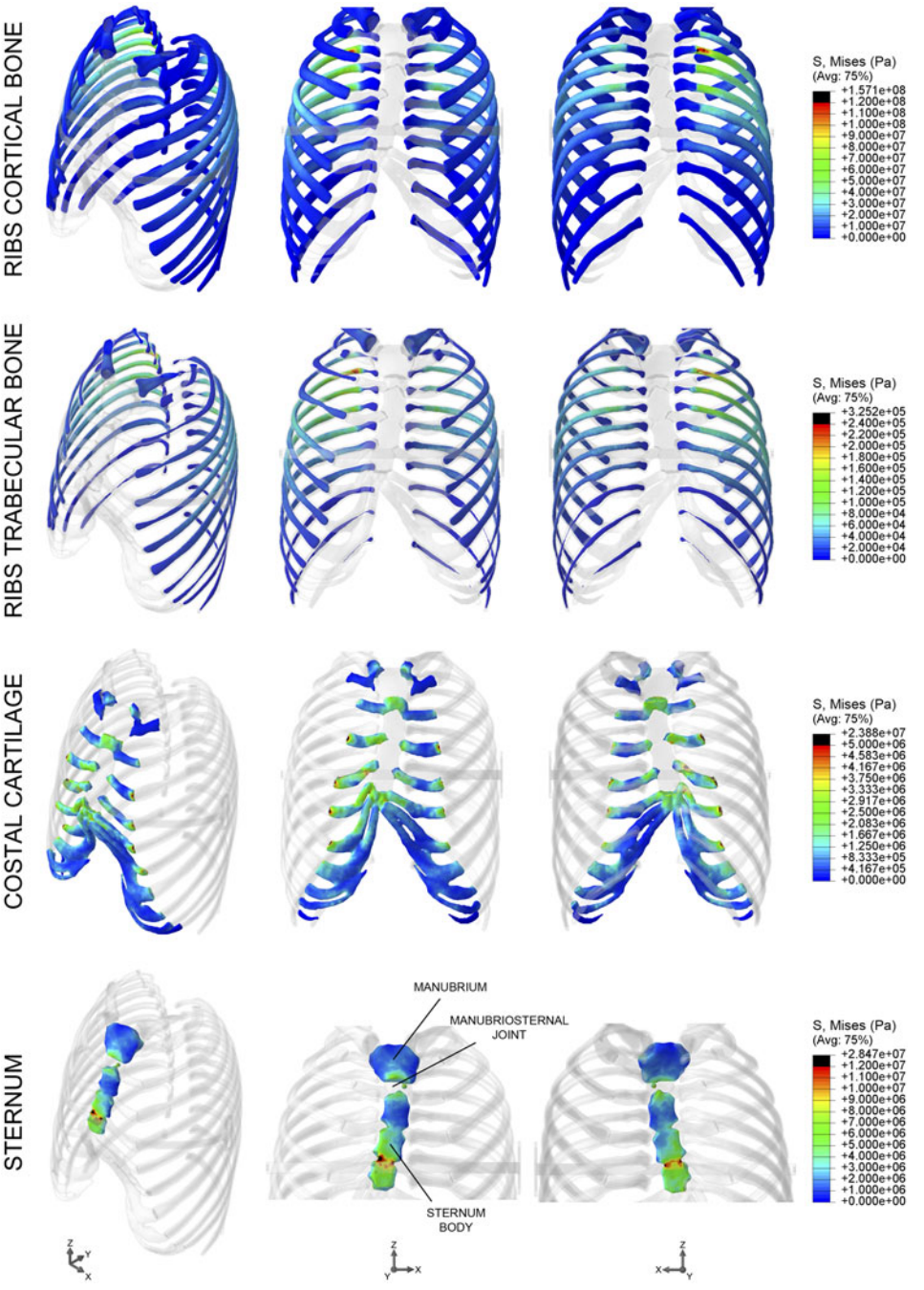

Figure 3. von Mises equivalent stress distribution on each different structure after the corrective procedure simulation.

scoliosis associated with PE and, as observed by Niedbala et al. (2003) and Nagasao et al. (2010), the thoracic scoliosis may be induced by the stress on the back of the ribs after the Nuss procedure. In a similar way, the 'reversed Nuss' procedure for the PC correction can also lead to induced scoliosis.

The bar displacement on the *yy*-axis is directly applied to the sternum and to the costal cartilage near it. The subsequent (indirect) displacement is transmitted to the ribs by the costal cartilages. Comparing the connective pairs of costal cartilage/ribs cortical bone and costal cartilage/sternum on the costal cartilages stress results (Figure 4), a higher stress is generated on the costal cartilage/ribs cortical bone connective pair due to the material properties and the aforementioned chain-like reaction.

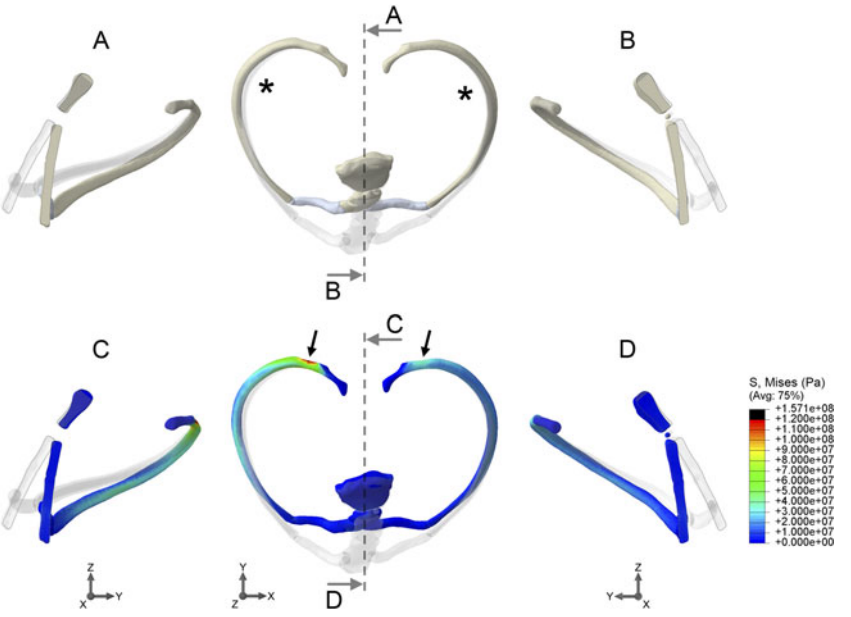

Figure 4. Detail of the 4th ribs, their corresponding costal cartilage portions and the sternum. The translucent colouring represents the state before the corrective procedure, and the normally coloured (top) and von Mises stress colouring (bottom) represent the state after the correction. The (∗) spots the regions where the ribs concavity was pronounced, and the arrows point out the areas where higher stress values were generated.

Table 3. Maximum von Mises stress values ($\times 10^6$ Pa) and maximum displacement values (magnitude and on each axis, in mm) of each rib cage structure after the corrective bar placement and fixation.

Structure	Maximum von Mises stress ($\times 10^6$ Pa)	Maximum displacement (mm)			
		Magnitude	U1 (*xx*)	U2 (*yy*)	U3 (*zz*)
Sternum bone	28.470	45.76	0.05	43.31	0.42
Costal cartilage	23.880	47.93	16.01	45.27	0.38
Ribs cortical bone	157.100	31.22	13.27	18.83	0.81
Ribs trabecular bone	0.325	30.63	12.94	18.06	0.65

The sternum position and its slight rotation (characteristic of *pectus* deformities) were almost completely corrected by the corrective procedure simulation (Figure 4). However, due to the cartilaginous tissue thickness on the manubriosternal joint (Figure 3), the manubrium alignment with the sternum body was less efficient.

It is agreed by physicians that, for the PC/PE correction through the MIS approach, the corrective bar must be placed, respectively, above/below the

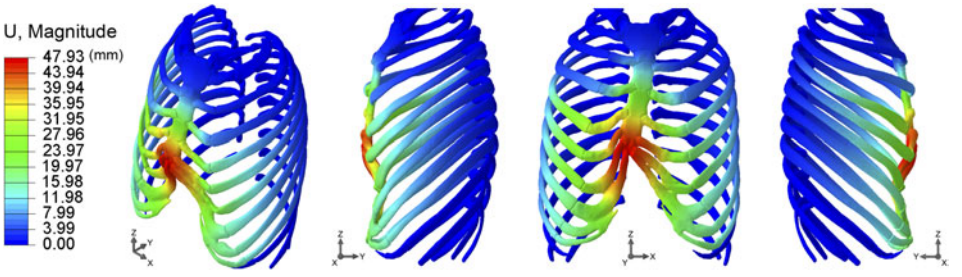

Figure 5. Rib cage model displacement magnitude distribution after the corrective procedure simulation.

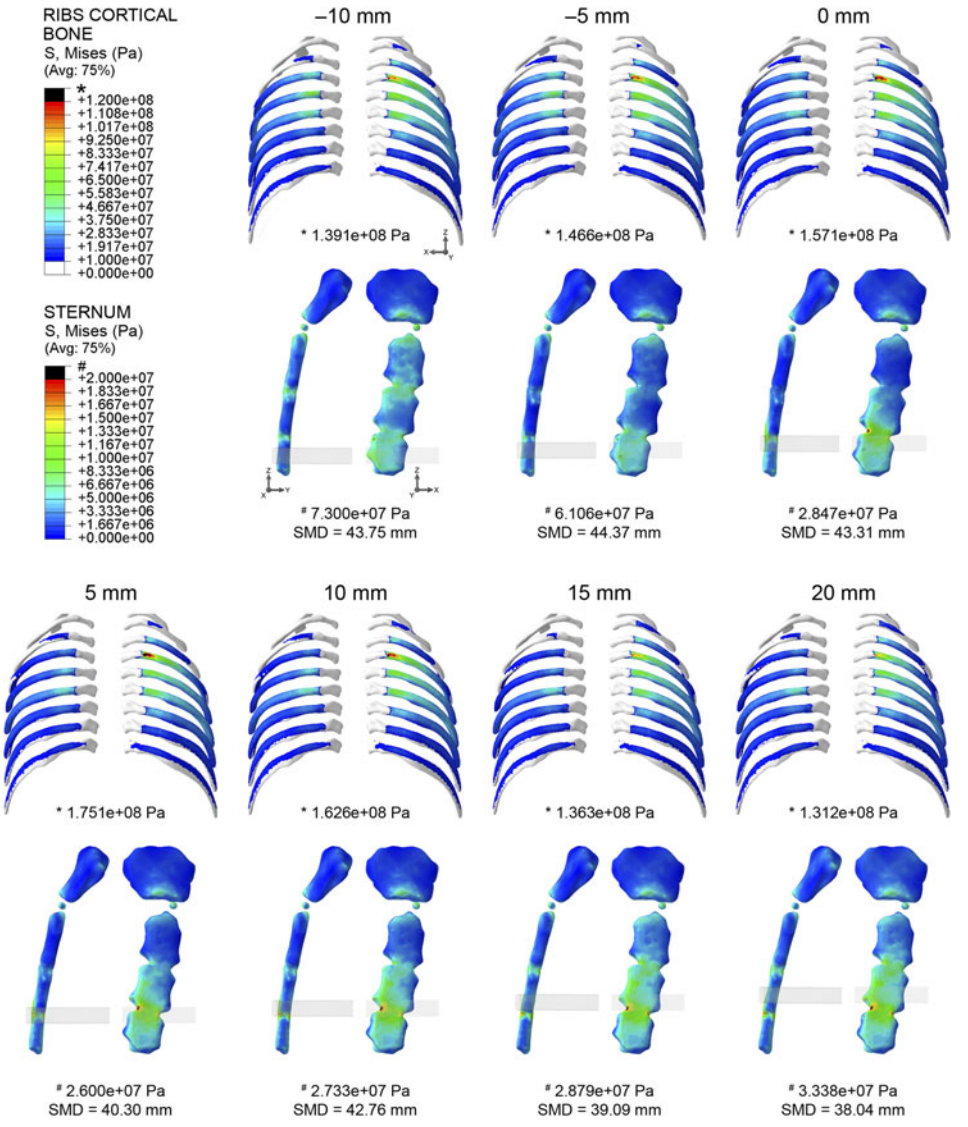

Figure 6. von Mises equivalent stress distribution on the 1st to 9th ribs cortical bone and sternum as a result of different bar positioning. Only the backend of the ribs are shown (*yy* plane view-cut). SMD stands for the sternum maximum displacement on the *yy*-axis.

sternum's most prominent region (Schaarschmidt et al. 2011; Yüksel et al. 2011). Thus, the relation between the corrective bar positioning along the sternum and the distribution of the stresses generated on the ribs' backend was investigated. As referred before, no direct relation can be established between the corrective bar positioning and the increase or decrease of the stresses generated on the ribs and sternum. As this corrective procedure occurs as a chain-like reaction, the costal cartilages play an important role on this phenomenon: they link the sternum to the ribs and they also exert pressure against the corrective bar. As can be observed in Figure 1, the costal cartilages are more prominent than the sternum and, consequently, the structures that first contact the bar. The corrective bar areas that contact the different thoracic cage components are also different for each bar position (Figure 7); this leads to different pressure values transmitted throughout the thoracic cage.

From the results presented in Figure 6, it can be observed that the 15 and 20 mm bar positions led to a less efficient sternum position correction (39 and 38 mm, respectively). However, the stresses generated on the ribs' backend for the 15- and 20-mm positions were less concentrated than those resulting from the remaining bar positions. Taking into account that the highest SCD difference is about 6 mm, this value can be negligible when compared to the importance on diminishing the ribs' backend stress and, consequently, the risk of PC correction-associated scoliosis.

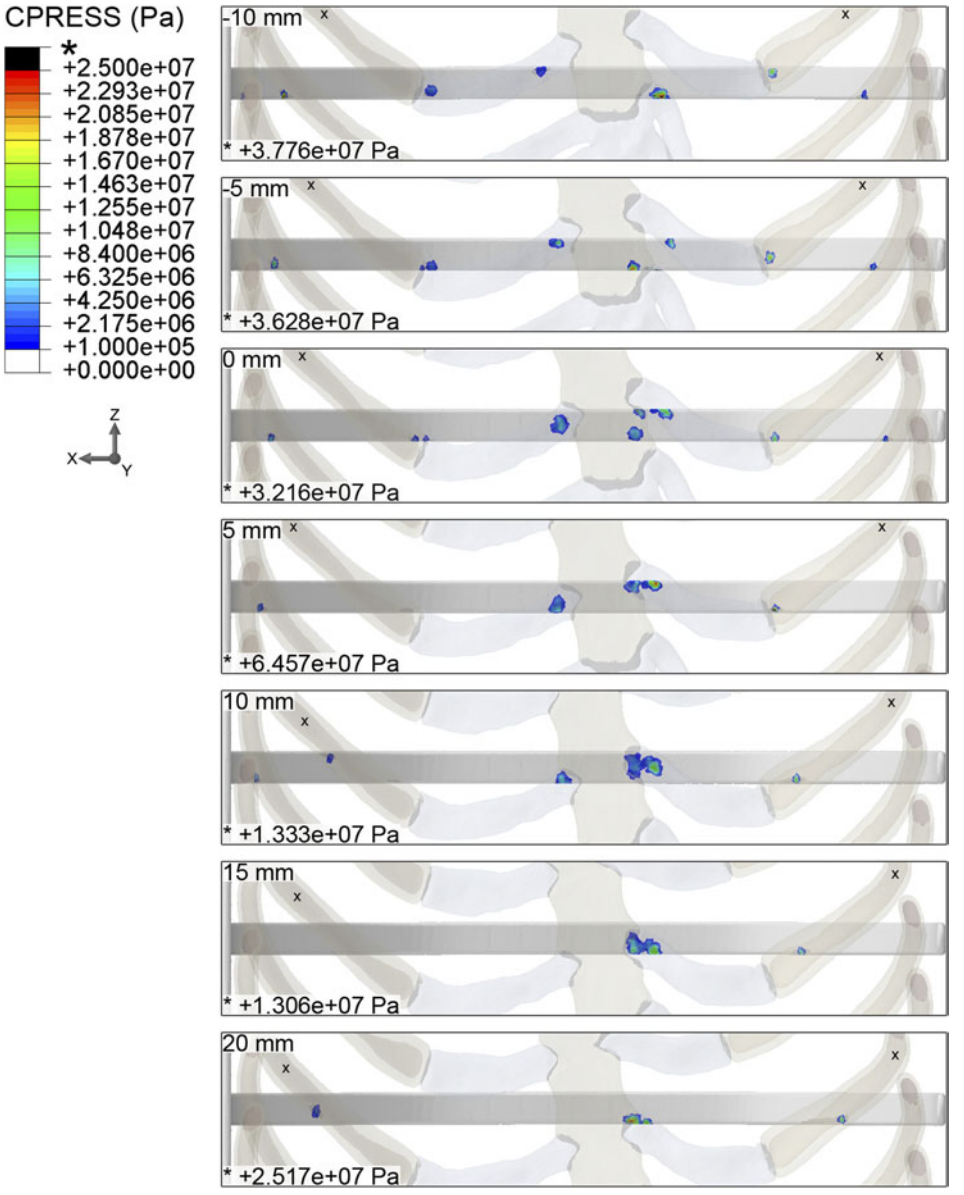

Figure 7. Corrective bar contact pressure sites and corresponding values according to the bar positioning. The (x) spots the 4th ribs.

5. Conclusions

This study represents the first biomechanical analysis of the minimally invasive modified Nuss procedure for the PC deformity correction, using a patient-specific modelled bar. Although aware that one of the main weaknesses of this study is the use of only one patient, we believe that the stresses generated on the ribs' extremities near the spine unveil the probable influence of PC corrective procedure on *pectus* corrections-associated scoliosis in all cases. The different bar positioning along the sternum influences the stresses generated on the ribs' backend. Thus, although the conventional positioning of the corrective bar over the most prominent region of the sternum leads to a higher sternum displacement, it may not be the most favourable positioning, leading to higher ribs' backend stresses. As our model lacks the complexity of the interactions between structures (muscles, ligaments, internal organs and spine), which play an important role on stress damping, the stress values presented in this study may be lower in real situations.

Fundings

This work was financially supported by the Portuguese Foundation for Science and Technology (FCT) under the R&D project PTDC/SAU-BEB/103368/2008 and the fellowship SFRH/BPD/46851/2008.

References

Abramson H, D'Agostino J, Wuscovi S. 2009. A 5-year experience with a minimally invasive technique for *pectus carinatum* repair. J Pediatr Surg. 44:118–123.

Awrejcewicz J, Łuczak B. 2006. Dynamics of the human thorax with the Lorenz *pectus* bar. In: Proceedings of the 22nd International Conference on Vibrations in Physical Systems; Apr 19–22; Poznań-Będlewo, Poland. p. 59–64.

Brodkin HA. 1958. Pigeon breast; congenital chondrosternal prominence; etiology and surgical treatment by xiphosternopexy. AMA Arch Surg. 77:261–270.

Chang PY, Hsu ZY, Chen DP, Lai JY, Wang CJ. 2008. Preliminary analysis of the forces on the thoracic cage of patients with *pectus excavatum* after the Nuss procedure. Clin Biomech. 23:881–885.

Coelho MS, Guimarães PSF. 2007. *Pectus carinatum*. J Bras Pneumol. 33:463–474.

Fang Q, Boas DA. 2009. Tetrahedral mesh generation from volumetric binary and grayscale images. In: Proceedings of the 6th IEEE International Symposium of Biomedical Imaging: from Nano to Macro; Jun 28 to Jul 1; Boston, MA, USA. p. 1142–1145.

Fonkalsrud EW. 2008. Surgical correction of *pectus carinatum*: lessons learned from 260 patients. J Pediatr Surg. 43:1235–1243.

Fonkalsrud EW, Beanes S. 2001. Surgical management of *pectus carinatum*: 30 years' experience. World J Surg. 25:898–903.

Fonkalsrud EW, Dunn JC, Atkinson JB. 2000. Repair of *pectus excavatum* deformities: 30 years of experience with 375 patients. Ann Surg. 231:443–448.

Hasan I, Heinemann F, Reimann S, Keilig L, Bourauel C. 2011. Finite element investigation of implant-supported fixed partial prosthesis in the premaxilla in immediately loaded and osseointegrated states. Comput Methods Biomech Biomed Eng. 14:979–985.

Hock A. 2009. Minimal access treatment of *pectus carinatum*: a preliminary report. Pediatr Surg Int. 25:337–342.

Jeon I, Bae J-Y, Park J-H, Yoon T-R, Todo M, Mawatari M, Hotokebuchi T. 2011. The biomechanical effect of the collar of a femoral stem on total hip arthroplasty. Comput Methods Biomech Biomed Eng. 14:103–112.

Jorge JP, Simões FM, Pires EB, Rego PA, Tavares DG, Lopes DS, Gaspar A. 2012. Finite element simulations of a hip joint with femoroacetabular impingement. Comput Methods Biomech Biomed Eng. [Epub ahead of print].

Kravarusic D, Dicken BJ, Dewar R, Harder J, Poncet P, Schneider M, Sigalet DL. 2006. The Calgary protocol for bracing of *pectus carinatum*: a preliminary report. J Pediatr Surg. 41:923–926.

Li Z, Kindig MW, Kerrigan JR, Untaroiu CD, Subit D, Crandall JR, Kent RW. 2010. Rib fractures under anterior–posterior dynamic loads: experimental and finite-element study. J Biomech. 43:228–234.

Nagasao T, Noguchi M, Miyamoto J, Jiang H, Ding W, Shimizu T, Kishi K. 2010. Dynamic effects of the Nuss procedure on the spine in asymmetric *pectus excavatum*. J Thorac Cardiovasc Surg. 140:1294–1299.e1291.

Niedbala A, Adams M, Boswell WC, Considine JM. 2003. Acquired thoracic scoliosis following minimally invasive repair of *pectus excavatum*. Am Surg. 69:530–533.

Nuss D, Croitoru DP, Kelly RE, Jr, Goretsky MJ, Nuss KJ, Gustin TS. 2002. Review and discussion of the complications of minimally invasive *pectus excavatum* repair. Eur J Pediatr Surg. 12:230–234.

Peña A, Pérez L, Nurko S, Dorenbaum D. 1981. *Pectus carinatum* and *pectus excavatum*: are they the same disease? Am Surg. 47:215–218.

Rack HJ, Qazi JI. 2006. Titanium alloys for biomedical applications. Mater Sci Eng C Mater Biol Appl. 26:1269–1277.

Schaarschmidt K, Lempe-Sellin M, Schlesinger F, Jaeschke U, Polleichtner S. 2011. New Berlin-Buch 'reversed Nuss,' endoscopic *pectus carinatum* repair using eight-hole stabilizers, submuscular CO_2, and presternal Nuss bar compression: first results in 35 patients. J Laparoendosc Adv Surg Tech A. 21:283–286.

Singh SV. 1980. Surgical correction of *pectus excavatum* and *carinatum*. Thorax. 35:700–702.

Vilaça JL, Marques Pinho AC, Correia-Pinto J, Fonseca JFC, Peixinho NRM. 2009. System for automatic and personalized modelling/bending of surgical prosthesis for correction of *pectus excavatum* based on pre-surgical imaging information. International Application Patent PCT/PT2008/000016376 filed April 24, 2008, and published March 19, 2009 (WO/2009/035358).

Waters P, Welch K, Micheli LJ, Shamberger R, Hall JE. 1989. Scoliosis in children with *pectus excavatum* and *pectus carinatum*. J Pediatr Orthop. 9:551–556.

Weber TR. 2005. Further experience with the operative management of asphyxiating thoracic dystrophy after *pectus* repair. J Pediatr Surg. 40:170–173.

Wei Y, Sun D, Liu P, Gao Y. 2010. *Pectus excavatum* nuss orthopedic finite element simulation. In: Proceedings of the 3rd International Conference on Biomedical Engineering and Informatics (BMEI); October 16–18; Yantai, China. p. 1236–1239.

Yüksel M, Bostanci K, Evman S. 2011. Minimally invasive repair of *pectus carinatum* using a newly designed bar and stabilizer: a single-institution experience. Eur J Cardiothorac Surg. 40:339–342.

Zhou ZR, Yu HY, Cai ZB, Zhu MH. 2005. Fretting behavior of cortical bone against titanium and its alloy. Wear. 259:910–918.